nature chemistry

ARTICLES

https://doi.org/10.1038/s41557-018-0010-2

Hydroxide diffuses slower than hydronium in water because its solvated structure inhibits correlated proton transfer

Mohan Chen[1,7], Lixin Zheng[1,7], Biswajit Santra[2], Hsin-Yu Ko[2], Robert A. DiStasio Jr[3], Michael L. Klein[1,4,5], Roberto Car[2,6*] and Xifan Wu[1,5*]

Proton transfer via hydronium and hydroxide ions in water is ubiquitous. It underlies acid–base chemistry, certain enzyme reactions, and even infection by the flu. Despite two centuries of investigation, the mechanism underlying why hydroxide diffuses slower than hydronium in water is still not well understood. Herein, we employ state-of-the-art density-functional-theory-based molecular dynamics—with corrections for non-local van der Waals interactions, and self-interaction in the electronic ground state—to model water and hydrated water ions. At this level of theory, we show that structural diffusion of hydronium preserves the previously recognized concerted behaviour. However, by contrast, proton transfer via hydroxide is less temporally correlated, due to a stabilized hypercoordination solvation structure that discourages proton transfer. Specifically, the latter exhibits non-planar geometry, which agrees with neutron-scattering results. Asymmetry in the temporal correlation of proton transfer leads to hydroxide diffusing slower than hydronium.

The anomalously high mobility of the hydronium, H_3O^+(aq), and hydroxide, OH^-(aq), ions solvated in water has fascinated scientists since the very beginning of molecular-based physical chemistry[1,2]. The two ions can be viewed as opposite topological defects in the fluctuating hydrogen-bond (H-bond) network in liquid water. In this picture, both ions bind to three water molecules by donating or accepting H-bonds. Diffusion is not dominated by hydrodynamics, but by a structural process usually referred to as the Grotthuss mechanism[3], in which a proton is transferred from a hydronium to a neighbouring water molecule or from a water molecule to a neighbouring hydroxide. In this process, a covalent O–H bond breaks while another forms as the topological defect jumps to an adjacent site in the network. Not surprisingly, proton transfer has been intensively investigated, both experimentally and theoretically, for almost a century since the early molecular models[4].

Although the Grotthuss mechanism correctly identifies the origin of fast diffusion, some issues remain unresolved. Experimentally, diffusivity is obtained via the Nernst equation from the measured electrical conductivity of the ions. While the diffusivity describes the combined effect of hydrodynamic and structural processes, the jump frequency of the protons in the structural process can be extracted from nuclear magnetic resonance (NMR) relaxation times. Conductivity[5–7] and NMR[5,8] experiments indicate that hydronium diffuses roughly twice as fast as hydroxide. Predicting the transfer dynamics is difficult as it depends on the cleavage and formation of covalent bonds in a fluctuating liquid medium. Major progress in modelling proton transfer came with the advent of ab initio molecular dynamics (AIMD)[9]. In this approach, the forces on the nuclei are derived from the instantaneous ground state of the electrons within density functional theory (DFT)[10,11], while the electrons adjust on the fly and can thereby access bond breaking and forming events. Importantly, the first AIMD study of hydronium and hydroxide in bulk water[12] showed that classical thermal fluctuations easily induce proton transfer events on the picosecond time scale.

In the case of hydronium, the first molecular simulations confirmed the long-held view that transfer involves interconversion of two defect complexes, that is, the solvated H_3O^+(aq) or Eigen ion[13,14], and the solvated $H_5O_2^+$(aq) or Zundel ion[15–23]. Even more notable were the results for hydroxide, OH^-(aq), which appeared to alternate between two configurations: an unexpected hypercoordinated form with four acceptor H-bonds and a nearly tetrahedral form with three acceptor H-bonds and, occasionally, a weak donor H-bond. Proton transfer only occurred in the latter configuration, suggesting a 'presolvation' mechanism, that is, access to the tetrahedral configuration, was necessary for proton transfer in OH^-(aq). Neutron diffraction[24] and core-level spectroscopy data[25] were consistent with the hypercoordinated structure, indirectly supporting the presolvation picture. However, analysis of neutron scattering data[24] suggested the solvation structure of OH^-(aq) had a pot-like shape, differing from the planar structure predicted by the early AIMD simulations[26], which employed the generalized gradient approximation (GGA) and treated nuclear dynamics classically. Subsequent path integral AIMD simulations, which treated the nuclei quantum mechanically, refined the model by stressing the fluxional character of the defect complexes, but did not change the basic picture as tunnelling was not found to be important[26,27]. In the latter scenario, proton transfer events occur randomly due to thermal and/or quantal fluctuations. However, recent AIMD simulations added a new twist to the story: proton transfer events are highly correlated and happen in bursts consisting of multiple jumps closely spaced in time followed by periods of inactivity[28,29].

[1]Department of Physics, Temple University, Philadelphia, PA, USA. [2]Department of Chemistry, Princeton University, Princeton, NJ, USA. [3]Department of Chemistry and Chemical Biology, Cornell University, Ithaca, NY, USA. [4]Department of Chemistry, Temple University, Philadelphia, PA, USA. [5]Institute for Computational Molecular Science, Temple University, Philadelphia, PA, USA. [6]Department of Physics, Princeton University, Princeton, NJ, USA. [7]These authors contributed equally: Mohan Chen, Lixin Zheng. *e-mail: rcar@princeton.edu; xifanwu@temple.edu

Table 1 | Computed ratios from the diffusion coefficients D (units: 10^{-9} m^2 s^{-1}) of H_3O^+(aq) (D^+) and OH^-(aq) (D^-), the experimental diffusivity data are computed from the limiting molar conductivities λ (units: Ω^{-1} cm^2 mol^{-1}) of H_3O^+(aq) (λ^+) and OH^-(aq) (λ^-) measured at 28 (refs [5,7]) and 25 °C (ref. [6])

	D^+	D^-	D^+/D^-
PW91	3.24	18.5	0.18
BLYP	2.83	1.92	1.47
HCTH/120	3.25	0.44	7.39
PBE	10.8±2.7	18.2±3.7	0.59±0.27
PBE-TS	12.8±1.9	8.3±1.6	1.54±0.53
PBE0-TS	8.3±1.9	3.7±0.4	2.24±0.75
Exp. (H_2O)	9.6[a], 9.4[c]	5.4[a], 5.2[c]	1.77[a], 1.80[c]
Exp. (D_2O)	6.9[a], 6.7[c]	3.2[a], 3.1[c]	2.15[a], 2.15[c]
	λ^+	λ^-	λ^+/λ^-
Exp. (H_2O)	364.0[a], 351[c]	206.0[a], 195[c]	1.77[a], 1.80[c]
Exp. (D_2O)	261.6[a], 252[c]	121.5[a], 117[c]	2.15[a], 2.15[c]
λ (H_2O)/ λ (D_2O)	1.39[a], 1.39[c], 1.364[b]	1.70[a], 1.67[c]	

The simulation data for six exchange-correlation functionals: PW91[57], BLYP[58,59], HCTH/120[60], PBE, PBE-TS and PBE0-TS, are reported. The data for the first three functionals are from ref. [26], those for the last three functionals are from the present simulation. We also show the standard deviations for computed D. The deuterium mass was used for both ions and water molecules in all AIMD simulations listed, while the experimental data (Exp.) based on both H and D are listed. See Supplementary Section 4 for more information on the procedures to compute diffusivities based on the AIMD simulations. The experimental diffusivity data were computed based on the Nernst equation $D = \frac{RT}{F^2}\lambda$, where R is the gas constant, T is the temperature, and F is Faraday's constant.
[a]from ref. [5]; [b]from ref. [6]; [c]from ref. [7].

The hypercoordinated hydroxide form revealed by previous simulations breaks the mirror symmetry of the topological defect model between hydronium and hydroxide. Yet, it is not evident why hydroxide diffuses slower than hydronium.

Previous simulations have adopted different flavours of the GGA for the exchange–correlation functional[26]. However, such GGAs not only overestimate the molecular polarizability and H-bond strength in liquid water, but also tend to grossly underestimate the equilibrium density of the liquid[30–32] by neglecting long-range van der Waals or dispersion interactions. More significantly, although the predicted diffusivities of H_3O^+(aq) are relatively stable from different GGA functionals, those for OH^-(aq) can vary by more than one order of magnitude[4,26,27,33] (Table 1). This large discrepancy inevitably hinders a proper comparison of diffusivities between the two ions.

Here we report AIMD simulations that adopt the hybrid functional PBE0[34,35] and include long-range van der Waals interactions using a self-consistent implementation of the Tkatchenko–Scheffler (TS)[36] scheme. The resulting PBE0-TS functional is less affected by the spurious self-interaction and better accounts for the molecular polarizability of water, greatly improving the overall description of neat water[37]. Our new data confirm the current picture of hydronium diffusion, namely proton transfers are highly correlated and occur with relatively high frequency. The effects of the functional approximation are much more pronounced in OH^-(aq), that is, hypercoordination increases, diffusivity decreases and the effect is accompanied by a strong suppression of multiple jumps. Double jumps are approximately four times more frequent than single jumps in the hydronium case, but they become slightly less frequent than single jumps for the hydroxide. We explain this behaviour as a consequence of the strongly amphiphilic character through a novel electronic structure analysis, making the lone pair side of OH^-(aq) more strongly hydrophilic and its H side more strongly hydrophobic. The diffusion constants of the two water ions and their ratio are in reasonable agreement with experiment.

Results and discussion

Proton transfer via the hydronium ion. The electronic structure of H_3O^+(aq) comprises three bonding electron pairs and one lone electron pair, which are represented by the maximally localized Wannier functions[39,40] in Fig. 1a. The protons of hydronium are positive and ready to be donated to neighbouring water molecules whereas the oxygen is likely to accept an H-bond from its neighbouring water molecules due to the negative lone electron pair. Since the H-bond is mainly attributed to an electrostatic attraction, the ability of donating (accepting) H-bonds can be conveniently measured by the distance separating the negative electrons from the positive nucleus, roughly estimating how positive (negative) the local environment is for a specific proton (oxygen). The resulting distance between electron pairs with respect to the nuclei, as obtained by the PBE0-TS trajectory, are shown in Fig. 1b for solvated ions and neat liquid water. Compared to liquid water, the proton of hydronium has a stronger ability to donate an H-bond, while the oxygen of hydronium has a weaker ability to receive one (Supplementary Section 2). Therefore, in the absence of proton transfers, the solvated hydronium is amphiphilic in nature with its proton (oxygen) site being hydrophilic (hydrophobic)[41–45]. Hence, H_3O^+(aq) forms the Eigen complex by stably donating three H-bonds to its neighbouring water molecules as shown in Fig. 1a. While supported by some experiments[46,47], this conventional picture has been challenged by recent experiments[17,21] suggesting that a long-lived Zundel complex plays a central role in proton solvation and transport. In the Zundel complex ($H_5O_2^+$(aq)) the excess proton has two flanking water molecules, called the special pair, which contribute prominently to the observed vibrational spectra. In the dynamic picture of AIMD simulations, however, there is no sharp distinction between Eigen and Zundel configurations. While waiting for a proton transfer event the solvated proton remains associated with a particular O atom but the corresponding complex keeps fluctuating through a continuum of structures including Eigen- and Zundel-like geometries. As demonstrated in a recent paper these structures contribute almost equally to the observed infrared and Raman vibrational signatures[23]. For illustrative purposes we adopt the conventional H_3O^+(aq) picture in the figures.

One proton of the hydronium can be transferred to a neighbouring water molecule, which in turn is converted to a new ion[12,48]. Moreover, proton transfers are highly correlated in time evidenced by the preferred bursts of proton transfer events to single proton transfer events[29]. In Fig. 2a–c, we report the frequencies of proton transfers categorized by the number (single, double, triple and quadruple) of transfer events during one burst. In general, the proton transfers obtained from the three AIMD trajectories (PBE, PBE-TS and PBE0-TS) are all dominated by concerted events with largely preferred double jumps. By analysing the PBE0-TS trajectory, we illustrate the free energy map in Fig. 3a with the length of water wire being a function of the proton transfer coordinate. The analysis confirms the recent discovery that double proton transfers are associated with the collective compression of a water wire[29]. This concerted behaviour enables the proton to diffuse rapidly through two or more water molecules within a single burst, which is enhanced when nuclear quantum effects (NQEs) are considered[49,50]. However, the H-bond network more physically modelled by the van der Waals interactions and exact exchange has non-negligible effects on the water wire compression and concerted proton transfers.

The van der Waals interaction, is an important effect causing denser water than ice under ambient conditions[31,32]. As in the case of pure water[37], the structure of the solution with ions is softened under the influence of van der Waals interactions. The increased population of water molecules in the interstitial region weakens the H-bond network, while leaving the strength of the short-range directional H-bonds unchanged. As expected, water wires in the

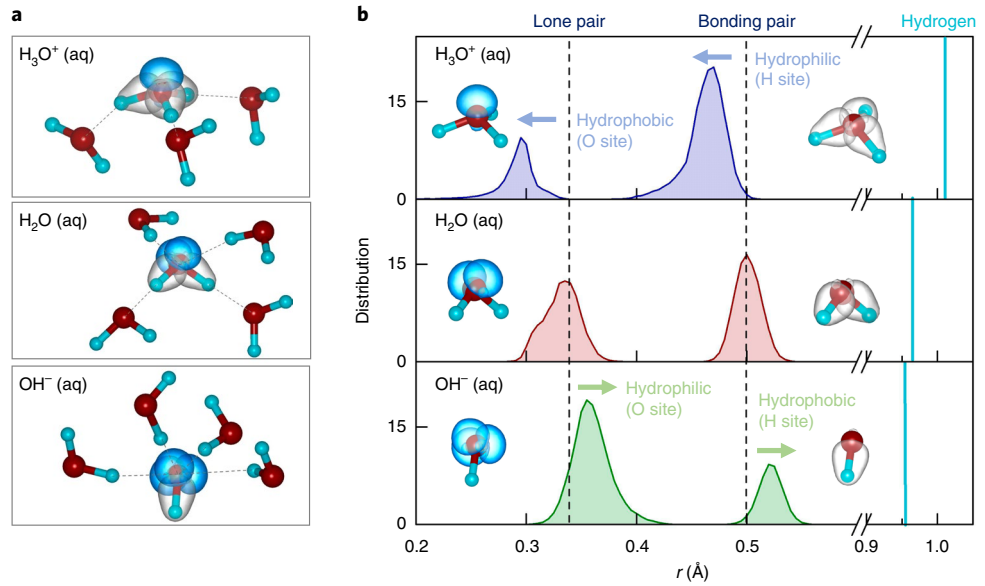

Fig. 1 | Electronic structure of the solvated water molecule and water ions from PBE0-TS trajectories. a, From top to bottom: solvation structures and maximally localized Wannier functions of H_3O^+(aq), H_2O(aq), and OH^-(aq). H_3O^+(aq) donates three H-bonds, H_2O(aq) accepts and, respectively, donates two H-bonds, OH^-(aq) accepts four H-bonds. Density isosurfaces of maximally localized Wannier functions for lone- and bonding-pair electrons are depicted in blue and grey, respectively. **b**, From top to bottom: distributions of the distances from the intramolecular oxygen of the maximally localized Wannier centres for H_3O^+(aq), H_2O(aq), and OH^-(aq). In each panel, the vertical cyan line indicates the average length of the covalent O–H bond,whereas the vertical dashed black line indicates the average distance from the intramolecular oxygen to the Wannier centres of lone and bonding pairs. The amphiphilic character of the ions emerges from the comparison with the neutral molecule: an ionic site, oxygen or hydrogen, is hydrophobic (hydrophilic) when the separation between the lone pair and oxygen, or between the bonding pair and hydrogen, is shorter (larger) than the corresponding distance in the neutral molecule.

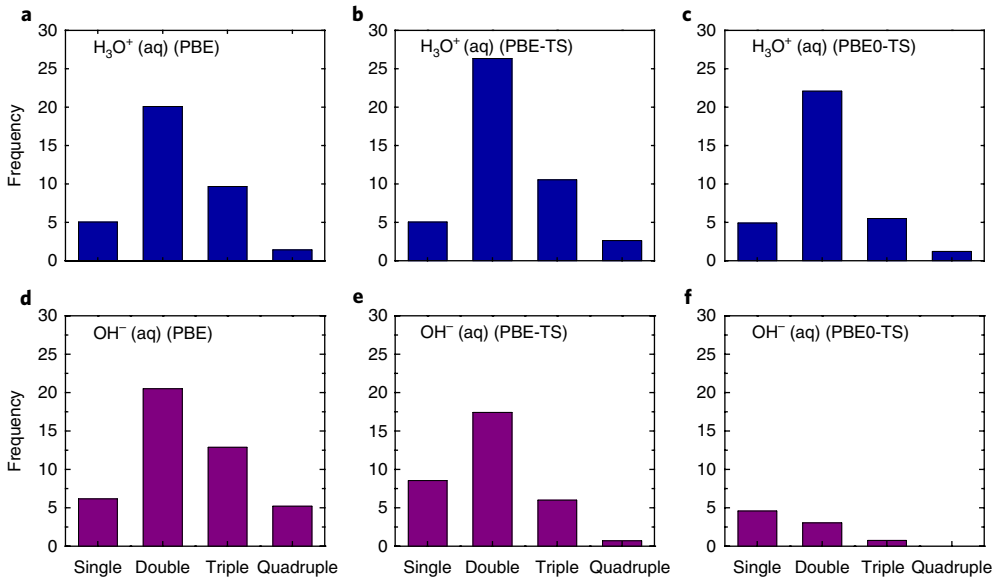

Fig. 2 | Frequency of proton transfer events with three exchange–correlation functionals (PBE, PBE-TS, and PBE0-TS). The blue bars show the frequency of single, double, triple and quadruple proton transfers for H_3O^+(aq). The purple bars show the frequency of single, double, triple and quadruple proton transfers for OH^-(aq). The frequency is calculated by counting the average number of proton transfers of each kind during a time span of 10 ps. Consecutive jumps separated in time by 0.5 ps or less contribute to multiple (that is, concerted) proton transfer events. A time lapse of 0.5 ps is the typical observed time scale of compression of a water wire. Events in which a proton returns to its original site within 0.5 ps are considered to be rattling fluctuations and are not included in these counts.

softer liquid structure described by PBE-TS can be compressed with a slightly shorter compression length of 0.487 Å compared with that of 0.502 Å in the PBE trajectory (Supplementary Section 3). The facilitated water wire compressions encourage more concerted proton transfers as shown in Fig. 2b. Consequently, the diffusivity increases as compared with the PBE trajectory (see Table 1).

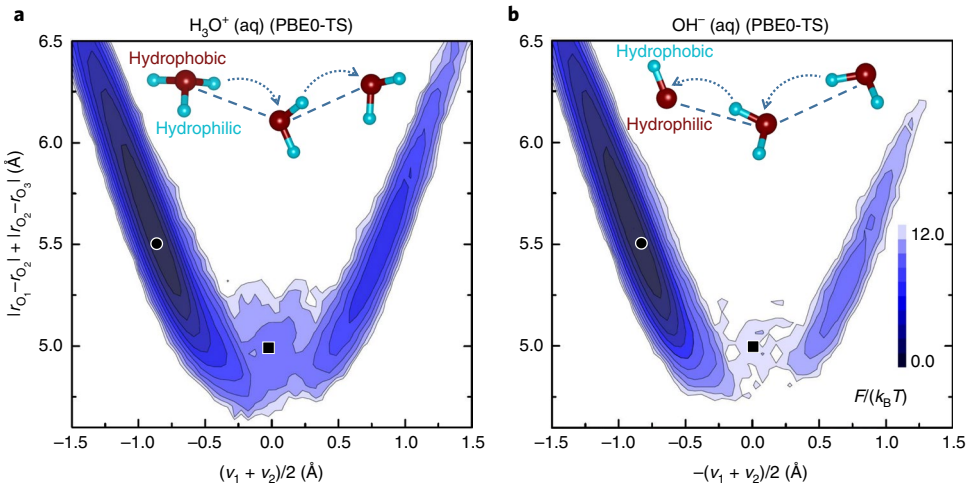

Fig. 3 | Free energy maps for water wire compression and double proton jumps with the PBE0-TS functional. The topographic map on the left is for H_3O^+(aq), the one on the right is for OH^-(aq). The map gives the isocontours of the free energy in the plane of two collective coordinates, $|r_{O(1)} - r_{O(2)}| + |r_{O(2)} - r_{O(3)}|$, describing the compression of a wire made by three neighbouring molecules, and $(v_1 + v_2)/2$ or $-(v_1 + v_2)/2$, describing the displacement of the two protons attempting a jump, as depicted schematically on top of each map. From left to right, the three oxygens have coordinates $r_{O(1)}$, $r_{O(2)}$ and $r_{O(3)}$, respectively, while the two protons have coordinates $r_{H(1)}$ and $r_{H(2)}$, respectively. The transfer coordinate is $v_1 = |r_{O(1)} - r_{H(1)}| - |r_{H(1)} - r_{O(2)}|$ for the first proton, and $v_2 = |r_{O(2)} - r_{H(2)}| - |r_{H(2)} - r_{O(3)}|$ for the second proton. Successful double jumps correspond to the configurations on the right of each map, that is, $v_1 + v_2 > 0$ for H_3O^+(aq) or $-(v_1 + v_2) > 0$ for OH^-(aq). All of the configurations in a trajectory of a three-water-wire, that is, a triplet of bonded molecules, are reported on the left of each map, but only a fraction of these configurations leads to a successful double jump. The free energy gives the relative probability of occurrence of the configurations in each map. The most stable configurations (left of the maps) are indicated by a black dot and the corresponding free energy is set equal to zero. The saddle points for double proton transfer are indicated by the black squares. The corresponding free energy barriers are 7.5 and 9.4 k_BT for H_3O^+(aq) and OH^-(aq), respectively. More details on barrier calculations are reported in Supplementary Section 3.

Electrons, as appropriately described by quantum mechanics, cannot interact with themselves. Yet, all conventional DFT functionals inherit self-interaction error, which artificially overestimates the H-bond strength[37]. Including fractional exact exchange in our PBE0-TS trajectories mitigates this self-interaction error. Compared with the van der Waals interactions, the exact exchange directly improves the overestimated H-bond strengths, which also affects the compression of water wire. The H-bond strengths among neighbouring water molecules become weaker resulting in a less polarizable liquid towards the experimental direction[37]. The reduced polarizability is mainly provided by the less negative electric environment of oxygen lone pair electrons[37]. The H-bonds binding hydronium to its three neighbouring water molecules are also weakened, as evidenced by the shorter distances between protons of the ion and their bonding electron pairs (0.542 Å in PBE0-TS compared to 0.550 Å in PBE-TS trajectories) yielding a less positive electric environment for protons (Supplementary Section 2). As a result, the water wire compression with weaker H-bonding becomes less easy as evidenced by the longer compression length of 0.562 Å compared to 0.487 Å in the PBE-TS trajectory (Supplementary Section 3). Consistently, slower hydronium diffusion in water is observed compared to that in the PBE-TS trajectory in Table 1. Thermal fluctuations give rise to a continuum of Eigen-like and Zundel-like configurations in all our simulations, consistent with previous findings[23,48]. The more localized protons with the hybrid functional slightly favour Eigen-like configurations but the distinction between Eigen and Zundel should be further blurred by inclusion of NQEs[48].

Proton transfer via the hydroxide ion. The OH^-(aq) ion is also amphiphilic[38] as determined by its electronic ground state in Fig. 1b. Based on the same criterion, we can conveniently determine the hydrophobicity and hydrophilicity of OH^-(aq) in Fig. 1b. The oxygen site of hydroxide is hydrophilic and more electronegative than the oxygen site of water, whereas the proton site of hydroxide is hydrophobic and less electropositive compared to the proton site in water (Supplementary Section 2). Although both OH^-(aq) and H_3O^+(aq) are amphiphilic, their electronic origins are different. The hydrophilicity of H_3O^+(aq) provided by its protons enables it to donate three H-bonds in the absence of proton transfer. In contrast, the hydrophilicity of OH^-(aq) provided by lone-pair electrons enables it to accept either three or four H-bonds, and both three- and hypercoordination solvation structures normally occur in the aqueous solution of OH^-(aq). The three-coordination solvation structure is tetrahedral-like and encourages proton transfers via the presolvation mechanism; while hypercoordination strongly disfavours proton transfers. Therefore, the mirror symmetry of the proton transfer mechanisms between the two ions is broken, and the proton transfer via hydroxide cannot be simply considered as the reverse process of the proton transfer via hydronium by replacing the proton with a 'proton hole'[26].

Interestingly, the proton transfers described by PBE0-TS not only become less frequent but also the relative contribution of multiple jumps is strongly reduced, as reported in Fig. 2f. This mechanism differs from the traditional view[29] based on GGA functionals, namely that proton transfers via OH^-(aq) should follow a similar trend as H_3O^+(aq), shown in Fig. 2d. While the proton transfers become less concerted, the diffusivity of OH^-(aq) also decreases relative to that of H_3O^+(aq), approaching a ratio that quantitatively agrees with the experimental value in Table 1.

The revised proton transfer mechanism for OH^-(aq) implies drastic changes brought by the van der Waals interactions and the hybrid functional, rather than perturbed water wires compression observed in the H_3O^+(aq) solution. Indeed, changes in the solvation structure of OH^-(aq) in Fig. 4d suggest substantially stabilized hypercoordination configurations. The PBE functional overestimates the polarizability, yielding over-structured water, and this over-strengthened tetrahedral H-bond network energetically favours the tetrahedral-like three-coordination, that is, the presolvated structure of OH^-(aq). Fig. 4d shows that PBE

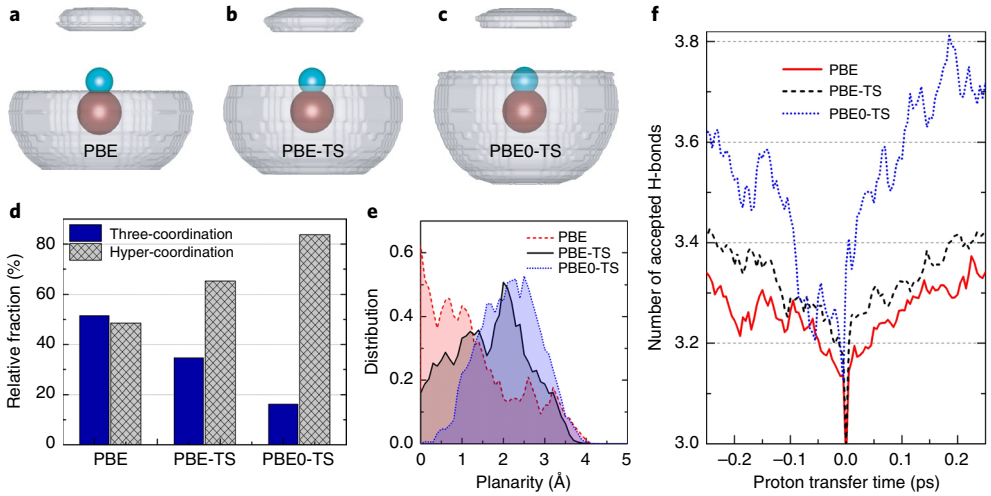

Fig. 4 | Solvation structures of OH^-(aq) with three functional approximations (PBE, PBE-TS, and PBE0-TS). a–c, Isosurfaces representing the spatial distribution of the oxygen sites of the solvating molecules in the hypercoordinated structure of OH^-(aq) with three functionals. The hydroxide ion has the hydrogen (cyan sphere) pointing upward and the oxygen (red sphere) pointing downward. **d**, Relative fraction of three- and hypercoordinated solvation structures with three functionals. In the three-coordinated structure OH^-(aq) accepts three H-bonds, in the hypercoordinated structure it accepts four H-bonds or more. **e**, Planarity distribution of the hypercoordinated structures with three functionals. The planarity order parameter is defined by the distance between a coordinating oxygen atom and the plane formed by three other coordinating oxygen atoms. **f**, Coordination number (number of acceptor H-bonds) of OH^-(aq) before ($t < 0$) and after ($t > 0$) a proton transfer event. Proton transfer events are very fast (~0.005 ps) on the time scale of the plot. Thus OH^-(aq) is always unambiguously defined and we can follow its evolution by adopting the Lagrangian point of view.

predicts 51% three-coordination and 49% hypercoordination. With the van der Waals interactions considered, the H-bond structure of liquid water is softened and facilitates the stabilization of hypercoordination of OH^-(aq). As a result, the percentage of hypercoordination increases from 49% in the PBE trajectory to 65% in the PBE-TS trajectory. The hypercoordination is further stabilized to 84% in the PBE0-TS trajectory. The additional amount of hyper-coordination (~19%) is attributed to two physical effects. As far as the H-bond network of the liquid solution is concerned, the exact exchange yields a weakened directional H-bond strength, and generates a further softened liquid water structure, which again helps to stabilize the hypercoordination structure. In the above, the weakened directional H-bond strength is mainly provided by a less negative environment of the lone pair electrons of liquid water, which is reduced by 2.9% (as measured by the distance between maximally localized Wannier centres and oxygen in Fig. 1). At short-range scale, the H-bonding between OH^-(aq) and the neighbouring waters is much less affected by the exact exchange than that of liquid water. The negative environment due to the lone pair electrons of the hydroxide is only reduced about 1.1%. As a result, the amphiphilic propensity of the solvated hydroxide is promoted, which enables the hydroxide to attract more water molecules further favouring the hypercoordination structure.

Conventional AIMD theories based on the GGA functionals repeatedly predicted a planar-like solvation structure of hypercoordinated OH^-(aq), that is, the four hydrogen-bonded water molecules accepted by OH^-(aq) roughly stay within a plane. We confirm in Fig. 4a that the distribution of water molecules surrounding OH^-(aq) is relatively flat from the PBE trajectory. The planar structure can be clearly demonstrated by the planarity (defined as the distance from one water to the plane formed by the other three water molecules) analysis shown in Fig. 4e, where the distribution of planarity centres at around zero indicating the dominant planar structure of hypercoordination. However, the experimental evidence based on the neutron scattering data[24] yields a non-planar solvation pattern.

In the PBE-TS and PBE0-TS trajectories, the H-bond network is modelled more accurately and the hypercoordination is stabilized. Therefore, more water molecules acquired by hypercoordination, are attracted to the first coordination shell. These additional water molecules are closer to the oxygen atom of OH^-,(aq) that is, a strongly hydrophilic site, and filling in the space close by. Consequently, the hypercoordination in the PBE0-TS trajectory exhibits a non-planar structure with its planarity distribution centered significantly away from zero in Fig. 4e. Furthermore, the surrounding water molecule density has a pot-like structure, shown in Fig. 4c, as found in the neutron scattering experiments[24]. The agreement strongly suggests that an accurate H-bond description, which has been achieved via PBE0-TS, is crucial to understand the proton transfer mechanism of OH^-(aq).

With more stabilized hypercoordination structures in OH^-(aq) from the PBE0-TS trajectory, the presolvated structure (three-coordination) of hydroxide becomes relatively rare. Therefore, the largely suppressed proton transfers in Fig. 2f are expected. However, it is intriguing that the majority of the suppressed proton transfers are of concerted types, while the frequency of single jump events is marginally influenced. The feature cannot be understood by the presolvation mechanism alone without considering the water wire compression. In this context, it is useful to compare the free-energy landscapes in Fig. 3a,b for the water wire compression as a function of the concerted (double) proton transfers coordinate. Consistently, it is found that the energy barrier for a double proton transfer to occur by the water wire compression in OH^-(aq) is about 1.9 k_BT larger than the similar energy barrier in H_3O^+(aq) (Supplementary Section 3). The significantly suppressed concerted proton transfers can be attributed to the energetically stabilized hypercoordination of OH^-(aq). Fig. 4f illustrates the changes of coordination number of OH^-(aq) with respect to the time before ($t < 0$) and after proton transfers ($t > 0$). Consistent with the presolvation mechanism, all simulations show OH^-(aq) relaxes from three-coordination back to the hypercoordination after each proton transfer event and vice versa. However, the more energetically stabilized hypercoordinated OH^-(aq) in the PBE0-TS trajectory

enables a much faster relaxation than that obtained from the PBE and PBE-TS trajectories. On average, the timescale of such relaxation in PBE0-TS trajectory is about 0.3 ps shorter than that of the typical water wire compression (~0.5 ps)[28]. The observed fast relaxation back to the hypercoordinated OH^-(aq) is a key to hinder the concerted proton transfer.

Conclusions

The origin of the different diffusion mechanisms of the hydrated water ions resides in their electronic ground states. Hence, an accurate theory of the solvent H-bond network is crucial. By utilizing state-of-the-art ab initio molecular dynamics, we confirmed proton transfers via the H_3O^+(aq) are frequent, with mostly concerted jumps. By contrast, proton transfers via the solvated hydroxide ion are more rare, with much fewer concerted jumps, due to the formation of (and rapid relaxation to) a stable non-planar and hypercoordinated solvation structure. This unique solvation shell, which is structurally consistent with neutron scattering experiments, actively discourages proton transfer in aqueous hydroxide solutions. Because the Stokes diffusions of these two water ions are roughly the same at the level of PBE0-TS theory, which are $(0.76 \pm 0.22) \times 10^{-9}$ and $(0.66 \pm 0.08) \times 10^{-9}\,m^2\,s^{-1}$ for H_3O^+(aq) and OH^-(aq), respectively, their differences in the nature of concerted proton transfers against simple proton transfer provide a rational explanation as to why hydroxide diffuses slower than hydronium in water. The different roles played by concerted proton transfer dynamics in H_3O^+(aq) and OH^-(aq) have direct bearing on the interpretation of the NMR experiments, which mostly assumed so far a simple Markovian process to extract the proton transfer rates[5,8]. NQEs play an important role in the dynamics of these two water ions; the concerted proton transfers will be further enhanced by the delocalized protons[50]. Our main conclusion is expected to be intact since previous studies suggested NQEs do not qualitatively affect the energetics of the solvation structures of the water ions. In this context, the extra stabilization of the hypercoordination structure of OH^-(aq) suggests a likely explanation for the large reported difference in the isotope effect on the transfer rates of the two aqua ions[8], as the deeper free energy well associated to OH^-(aq) in our simulation should translate in a comparatively larger quantum zero-point motion effect in OH^-(aq) than in H_3O^+(aq).

Methods

We used the Quantum ESPRESSO[51] software to perform simulations based on density functional theory. We used a method[35] based on Wannier functions to compute efficiently exact exchange in PBE0 calculations, and evaluated self-consistently[37] the TS dispersion contribution. The pure water system is composed of 128 H_2O. The hydronium system consists of 63 H_2O with one excess proton (127 H atoms and 63 O atoms) whereas the hydroxide system consists of 63 H_2O with one hydroxide ion (127 H atoms and 64 O atoms). In order to reproduce the experimental density of liquid water at ambient conditions, the cubic cells used for ion and pure water simulations have the cell lengths 12.4 and 15.7 Å, respectively. Only the gamma point was used to sample the Brillouin zone of the supercell. The periodic boundary conditions were utilized with the energy cutoff of plane wave basis being 72 Ry. Troullier–Martins[52] norm-conserving pseudopotentials were employed.

We performed the Car–Parrinello molecular dynamics[9] with the standard Verlet algorithm to propagate nuclear and electronic degrees of freedom. We used a fictitious electronic mass of 150 a.u. to ensure the adiabatic separation between the nuclear and electronic degrees of freedom, and the mass preconditioning with a kinetic energy cutoff of 6 Ry was applied to all Fourier components of electronic wave functions[53]. All simulations were performed in the NVT ensemble at 330 K (ref. [37]). The ionic temperature was controlled using the Nosé–Hoover chain thermostats[54] with one Nosé–Hoover chain per atom and four thermostats in each chain. The time step was set to be 3.5 a.u. (~0.08 fs). The nuclear mass of deuterium (2.0135 a.m.u.) was set for each hydrogen atom to accelerate the convergence, while the nuclear mass of oxygen was set to 15.9995 a.m.u. We generated 28-, 45- and 32-ps trajectories for the hydronium systems using the Perdew–Burke–Ernzerhof (PBE)[55]; PBE with the van der Waals interactions in the form of Tkatchenko and Scheffler[36] (PBE-TS); and PBE-TS with a mixing of 25 per cent exact exchange[34] (PBE0-TS) functionals, respectively; we also generated 54-, 55- and 38-ps for the hydroxide systems using the PBE, PBE-TS, and PBE0-TS functionals, respectively. For the pure liquid water system, we have trajectories of 14, 14 and 25 ps for PBE, PBE-TS, and PBE0-TS trajectories, respectively. We defined the H-bond within a cutoff of 3.5 Å for O–O distance and an H–O–O angle less than 30° (ref. [56]). We also used a cutoff of 1.24 Å for the O–H covalent bond.

Data availability. The data that support the findings of this study are available from the corresponding authors upon reasonable request.

Received: 2 October 2017; Accepted: 23 January 2018;
Published online: 12 March 2018

References

1. Hückel, E. 3. Einzelvorträge: elektrochemie. theorie der beweglichkeiten des wasserstoff-und hydroxylions in wässriger lösung. *Z. Elektrochem. Angew. Phys. Chem.* **34**, 546–562 (1928).
2. Bernal, J. & Fowler, R. A theory of water and ionic solution, with particular reference to hydrogen and hydroxyl ions. *J. Phys. Chem.* **1**, 515–548 (1933).
3. de Grotthuss, C. Theory of decomposition of liquids by electrical currents. [in French] *Ann. Chim.* **58**, 54–74 (1806).
4. Agmon, N. et al. Protons and hydroxide ions in aqueous systems. *Chem. Rev.* **116**, 7642–7672 (2016).
5. Halle, B. & Karlström, G. Prototropic charge migration in water. Part 2. Interpretation of nuclear magnetic resonance and conductivity data in terms of model mechanisms. *J. Chem. Soc. Faraday Trans. 2* **79**, 1047–1073 (1983).
6. Weingärtner, H. & Chatzidimttriou-Dreismann, C. Anomalous H^+ and D^+ conductance in H_2O–D_2O mixtures. *Nature* **346**, 548–550 (1990).
7. Sluyters, J. & Sluyters-Rehbach, M. The mechanism of the hydrogen ion conduction in liquid light and heavy water derived from the temperature dependence of their limiting conductivities. *J. Phys. Chem. B* **114**, 15582–15589 (2010).
8. Halle, B. & Karlström, G. Prototropic charge migration in water. Part 1. Rate constants in light and heavy water and in salt solution from oxygen-17 spin relaxation. *J. Chem. Soc. Faraday Trans. 2* **79**, 1031–1046 (1983).
9. Car, R. & Parrinello, M. Unified approach for molecular dynamics and density-functional theory. *Phys. Rev. Lett.* **55**, 2471 (1985).
10. Hohenberg, P. & Kohn, W. Inhomogeneous electron gas. *Phys. Rev.* **136**, B864–B871 (1964).
11. Kohn, W. & Sham, L. J. Self-consistent equations including exchange and correlation effects. *Phys. Rev.* **140**, A1133–A1138 (1965).
12. Tuckerman, M. E., Laasonen, K., Sprik, M. & Parrinello, M. Ab initio simulations of water and water ions. *J. Phys. Condens. Matter* **6**, A93 (1994).
13. Wicke, E., Eigen, M. & Ackermann, T. Über den zustand des protons (hydroniumions) in wäβriger lösung. *Z. Phys. Chem.* **1**, 340 (1954).
14. Eigen, M. Proton transfer, acid–base catalysis, and enzymatic hydrolysis. Part I: Elementary processes. *Angew. Chem. Int. Ed.* **3**, 1–19 (1964).
15. Zundel, G. & Metzger, H. Energiebänder der tunnelnden überschuß-protonen in flüssigen säuren. Eine IR-spektroskopische untersuchung der natur der gruppierungen $H_5O_2^+$. *Z. Phys. Chem.* **58**, 225–245 (1968).
16. Tse, Y.-L. S., Knight, C. & Voth, G. A. An analysis of hydrated proton diffusion in ab initio molecular dynamics. *J. Chem. Phys.* **142**, 014104 (2015).
17. Thämer, M., De Marco, L., Ramasesha, K., Mandal, A. & Tokmakoff, A. Ultrafast 2D IR spectroscopy of the excess proton in liquid water. *Science* **350**, 78–82 (2015).
18. Decka, D., Schwaab, G. & Havenith, M. A. THz/FTIR fingerprint of the solvated proton: evidence for Eigen structure and Zundel dynamics. *Phys. Chem. Chem. Phys.* **17**, 11898–11907 (2015).
19. Dahms, F. et al. The hydrated excess proton in the Zundel cation $H_5O_2^+$: the role of ultrafast solvent fluctuations. *Angew. Chem. Int. Ed.* **55**, 10600–10605 (2016).
20. Wolke, C. T. et al. Spectroscopic snapshots of the proton-transfer mechanism in water. *Science* **354**, 1131–1135 (2016).
21. Dahms, F., Fingerhut, B. P., Nibbering, E. T., Pines, E. & Elsaesser, T. Large-amplitude transfer motion of hydrated excess protons mapped by ultrafast 2D IR spectroscopy. *Science* **357**, 491–495 (2017).
22. Biswas, R., Carpenter, W., Fournier, J. A., Voth, G. A. & Tokmakoff, A. IR spectral assignments for the hydrated excess proton in liquid water. *J. Phys. Chem.* **146**, 154507 (2017).
23. Daly, C. A. et al. Decomposition of the experimental Raman and infrared spectra of acidic water into proton, special pair, and counter-ion contributions. *J. Phys. Chem. Lett.* **8**, 5246–5252 (2017).
24. Botti, A., Bruni, F., Imberti, S., Ricci, M. & Soper, A. Solvation of hydroxyl ions in water. *J. Phys. Chem.* **119**, 5001–5004 (2003).
25. Aziz, E. F., Ottosson, N., Faubel, M., Hertel, I. V. & Winter, B. Interaction between liquid water and hydroxide revealed by core–hole de-excitation. *Nature* **455**, 89–91 (2008).
26. Tuckerman, M. E., Chandra, A. & Marx, D. Structure and dynamics of OH^-(aq). *Acc. Chem. Res.* **39**, 151–158 (2006).

27. Marx, D. Proton transfer 200 years after von Grotthuss: insights from ab initio simulations. *ChemPhysChem* **7**, 1848–1870 (2006).
28. Hassanali, A., Prakash, M. K., Eshet, H. & Parrinello, M. On the recombination of hydronium and hydroxide ions in water. *Proc. Natl Acad. Sci. USA* **108**, 20410–20415 (2011).
29. Hassanali, A., Giberti, F., Cuny, J., Kühne, T. D. & Parrinello, M. Proton transfer through the water gossamer. *Proc. Natl Acad. Sci. USA* **110**, 13723–13728 (2013).
30. Gillan, M. J., Alfè, D. & Michaelides, A. Perspective: how good is DFT for water? *J. Phys. Chem.* **144**, 130901 (2016).
31. Gaiduk, A. P., Gygi, F. & Galli, G. Density and compressibility of liquid water and ice from first-principles simulations with hybrid functionals. *J. Phys. Chem. Lett.* **6**, 2902–2908 (2015).
32. Miceli, G., de Gironcoli, S. & Pasquarello, A. Isobaric first-principles molecular dynamics of liquid water with nonlocal van der Waals interactions. *J. Chem. Phys.* **142**, 034501 (2015).
33. Marx, D., Chandra, A. & Tuckerman, M. E. Aqueous basic solutions: hydroxide solvation, structural diffusion, and comparison to the hydrated proton. *Chem. Rev.* **110**, 2174–2216 (2010).
34. Perdew, J. P., Ernzerhof, M. & Burke, K. Rationale for mixing exact exchange with density functional approximations. *J. Phys. Chem.* **105**, 9982–9985 (1996).
35. Wu, X. F., Selloni, A. & Car, R. Order-N implementation of exact exchange in extended insulating systems. *Phys. Rev. B* **79**, 085102 (2009).
36. Tkatchenko, A. & Scheffler, M. Accurate molecular van der Waals interactions from ground-state electron density and free-atom reference data. *Phys. Rev. Lett.* **102**, 073005 (2009).
37. DiStasio, R. A. Jr, Santra, B., Li, Z., Wu, X. & Car, R. The individual and collective effects of exact exchange and dispersion interactions on the ab initio structure of liquid water. *J. Phys. Chem.* **141**, 084502 (2014).
38. Crespo, Y. & Hassanali, A. Unveiling the Janus-like properties of OH^-. *J. Phys. Chem. Lett.* **6**, 272–278 (2015).
39. Marzari, N. & Vanderbilt, D. Maximally localized generalized Wannier functions for composite energy bands. *Phys. Rev. B* **56**, 12847–12865 (1997).
40. Marzari, N., Mostofi, A. A., Yates, J. R., Souza, I. & Vanderbilt, D. Maximally localized Wannier functions: theory and applications. *Rev. Mod. Phys.* **84**, 1419 (2012).
41. Hassanali, A. A., Giberti, F., Sosso, G. C. & Parrinello, M. The role of the umbrella inversion mode in proton diffusion. *Chem. Phys. Lett.* **599**, 133–138 (2014).
42. Wang, F., Izvekov, S. & Voth, G. A. Unusual "amphiphilic" association of hydrated protons in strong acid solution. *J. Am. Chem. Soc.* **130**, 3120–3126 (2008).
43. Iuchi, S., Chen, H., Paesani, F. & Voth, G. A. Hydrated excess proton at water–hydrophobic interfaces. *J. Phys. Chem. B* **113**, 4017–4030 (2008).
44. Tse, Y. L., Chen, C., Lindberg, G. E., Kumar, R. & Voth, G. A. Propensity of hydrated excess protons and hydroxide anions for the air–water interface. *J. Am. Chem. Soc.* **137**, 12610 (2015).
45. Giberti, F. & Hassanali, A. The excess proton at the air–water interface: the role of instantaneous liquid interfaces. *J. Chem. Phys.* **146**, 244703 (2017).
46. Woutersen, S. & Bakker, H. J. Ultrafast vibrational and structural dynamics of the proton in liquid water. *Phys. Rev. Lett.* **96**, 138305 (2006).
47. Tielrooij, K. J., Timmer, R. L. A., Bakker, H. J. & Bonn, M. Structure dynamics of the proton in liquid water probed with terahertz time-domain spectroscopy. *Phys. Rev. Lett.* **102**, 198303 (2009).
48. Marx, D., Tuckerman, M. E., Hutter, J. & Parrinello, M. The nature of the hydrated excess proton in water. *Nature* **397**, 601–604 (1999).
49. Chen, J., Li, X.-Z., Zhang, Q., Michaelides, A. & Wang, E. Nature of proton transport in a water-filled carbon nanotube and in liquid water. *Phys. Chem. Chem. Phys.* **15**, 6344–6349 (2013).
50. Giberti, F., Hassanali, A. A., Ceriotti, M. & Parrinello, M. The role of quantum effects on structural and electronic fluctuations in neat and charged water. *J. Phys. Chem. B* **118**, 13226–13235 (2014).
51. Giannozzi, P. et al. Advanced capabilities for materials modelling with Quantum ESPRESSO. *J. Phys. Condens. Matter* **29**, 465901 (2017).
52. Troullier, N. & Martins, J. L. Efficient pseudopotentials for plane-wave calculations. *Phys. Rev. B* **43**, 1993–2006 (1991).
53. Tassone, F., Mauri, F. & Car, R. Acceleration schemes for ab initio molecular-dynamics simulations and electronic-structure calculations. *Phys. Rev. B* **50**, 10561 (1994).
54. Martyna, G. J., Klein, M. L. & Tuckerman, M. E. Nosé–Hoover chains: the canonical ensemble via continuous dynamics. *J. Phys. Chem.* **97**, 2635–2643 (1992).
55. Perdew, J. P., Burke, K. & Ernzerhof, M. Generalized gradient approximation made simple. *Phys. Rev. Lett.* **77**, 3865 (1996).
56. Luzar, A. & Chandler, D. Hydrogen-bond kinetics in liquid water. *Nature* **379**, 55–57 (1996).
57. Wang, Y. & Perdew, J. P. Correlation hole of the spin-polarized electron gas, with exact small-wave-vector and high-density scaling. *Phys. Rev. B* **44**, 13298 (1991).
58. Becke, A. D. Density-functional exchange-energy approximation with correct asymptotic behavior. *Phys. Rev. A* **38**, 3098 (1988).
59. Lee, C., Yang, W. & Parr, R. G. Development of the Colle–Salvetti correlation–energy formula into a functional of the electron density. *Phys. Rev. B* **37**, 785 (1988).
60. Boese, A. D., Doltsinis, N. L., Handy, N. C. & Sprik, M. New generalized gradient approximation functionals. *J. Phys. Chem.* **112**, 1670–1678 (2000).

Acknowledgements

This project was supported by US Department of Energy SciDAC under grant numbers DE-SC0008726 and DE-SC0008626 and partially supported by the Division of Materials Research (DMR) under Award DMR-1552287. R.A.D. acknowledges partial support from Cornell University through start-up funding and the Cornell Center for Materials Research (CCMR) with funding from the National Science Foundation (NSF) MRSEC programme (DMR-1719875). This research used resources of the Argonne Leadership Computing Facility at Argonne National Laboratory, which is supported by the Office of Science of the US Department of Energy under contract number DE-AC02-06CH11357. This research also used resources of the National Energy Research Scientific Computing Center, which is supported by the Office of Science of the US Department of Energy under contract number DE-AC02-05CH11231. X.W. is grateful for the useful discussions with D. Vanderbilt at Rutgers University and A. J. Shanahan at University Medical Center of Princeton.

Author contributions

X.W., R.C. and M.L.K. designed the project. M.C. and L.Z. carried out the simulations. M.C. and L.Z. performed the analysis. R.A.D., B.S. and H.-Y.K. developed methodologies in Quantum ESPRESSO. X.W., R.C., M.L.K. and R.A.D. wrote the manuscript. All authors contributed to the discussions and revisions of the manuscript.

Competing interests

The authors declare no competing interests.

Additional information

Supplementary information is available for this paper at https://doi.org/10.1038/s41557-018-0010-2.

Reprints and permissions information is available at www.nature.com/reprints.

Correspondence and requests for materials should be addressed to R.C. and X.W.

Publisher's note: Springer Nature remains neutral with regard to jurisdictional claims in published maps and institutional affiliations.